PERGAMON

International Journal of Multiphase Flow 27 (2001) 89–105

International Journal of Multiphase Flow

www.elsevier.com/locate/ijmulflow

Behavior of particles and bubbles around immersed tubes in a fluidized bed at high temperature and pressure: a DEM simulation

Degang Rong, Masayuki Horio*

Department of Chemical Engineering, BASE, Tokyo University of Agriculture and Technology, Koganei, Tokyo, 184-8588 Japan

Received 24 June 1999; received in revised form 29 December 1999

Abstract

Numerical simulations were carried out to investigate the behavior of particles and bubbles around immersed tubes in a two-dimensional fluidized bed at elevated pressures. Bed temperature was kept constant at 850°C and bed pressure was varied from 0.1 to 1.2 MPa. The particle–tube impact velocity and impact angle, the number of particle–tube impacts and the bed voidage around tubes in a staggered tube bank were calculated. It was found that the bed expansion height increased with the increasing pressure both at constant u_0/u_{mf} and $u_0 - u_{mf}$. Under elevated pressure, 1.2 MPa, the bubble frequency was about 4–8 Hz which was slightly higher than 2–4 Hz for the ambient condition, and the time-averaged velocity of particle–tube impacts at tube bottom area was also higher than that under the ambient pressure. The average particle–tube impact velocity showed its maximum at 10–70° from the tube bottom. The time average of bed voidage around a tube increased with the increasing pressure. The distributions of bed voidage and particle–tube impact velocity around a tube were asymmetrical, which may be due to the local bubble habits. The tube erosion rate was predicted to be 7.9–19.4 μm/1000 h and the maximum erosion occurred at ambient pressure because of the large amount of particle–tube impacts.

Keywords: Fluidized bed; Particles and bubbles; Immersed tubes; High temperature; Elevated pressure; DEM simulation

* Corresponding author. Tel.: +81-423-86-3303; fax: +81-423-86-3303.
E-mail address: masa@cc.tuat.ac.jp (M. Horio).

0301-9322/01/$ - see front matter
PII: S0301-9322(00)00003-3

1. Introduction

Pressurized fluidized bed (PFB) combustion is one of the clean coal technologies to utilize coal cleanly and generate electricity with a higher efficiency. In a PFB combustor, bed materials (coal, absorbent and inert particles) are fluidized in a bubbling mode. Tubes immersed in the bubbling region absorb heat from particles and gases. On the other hand, they experience erosion and abrasion caused by particle attack on them. To improve heat transfer and reduce erosion rate, it is of great importance to get information on particle and bubble motion near immersed tubes at high temperature and pressure.

During the past few decades, gas–solid fluidization at high temperatures and pressures has been extensively investigated. However, the effect of pressure on the motion of particles and bubbles is still not well understood, especially for those cases with immersed tubes at high temperature. This is probably due to the lack of effective measuring technique and the high cost of experiments (under high temperatures and pressures).

Here, let us briefly review the previous studies on the high temperature and pressure effects upon bubbling fluidization, especially for those cases with particles near Geldart B/D boundary in which the bed materials of PFB combustors are found. In most of these studies, temperature and pressure effects were investigated separately for cases without tubes.

Mii et al. (1973) examined temperature effect up to 800°C and found that the bubble frequency increased with the increasing temperature at ambient pressure. Similar results were obtained by Yoshida et al. (1974) and Otake et al. (1975). However, the criterion for comparison was not discussed.

Botterill and Desai (1972) investigated the fluidization characteristics at elevated pressures and observed that the fluidization became smoother as bed pressures increased from 0.1–1 MPa. Knowlton (1977) also reported similar phenomena occurring at elevated pressures 1–7 MPa.

Kawabata et al. (1981) did their experiments by using a two-dimensional bed of 300×10 mm^2 in bed cross-section and observed that bubbles became flatter as bed pressures increased from 0.1–0.8 MPa. Rowe et al. (1983) also reported the same tendency for up to 8 MPa and further found that bubble behavior typical to Geldart group B at low pressures showed group A behavior at high pressures.

Hoffman and Yates (1986) reported that the bubble stability and maximum bubble size decreased at high pressures (up to 8 MPa) in their experiments. This is consistent with the observation by Chan et al. (1987).

Olowson and Almstedt (1990) studied bubble behavior by operating a bed at pressures up to 1.6 MPa and found that mean bubble frequency, mean bubble rise velocity and mean bubble volume fraction increased with the bed pressure while pierced bubble length decreased.

For a fluidized bed containing a tube bank, Olsson et al. (1995) investigated the influence of pressure, fluidization velocity and the tube bank geometry on bubble behavior and gas flow distribution. The bed had a cross-section of 0.2×0.3 m^2 and the bed material was 0.7 mm silica sand. Bed pressure was varied from 0.1 to 1.6 Mpa, while excess gas velocity was kept constant (0.2 and 0.6 m/s). They found that the bed expansion, bubble volume fraction and visible bubble flow-rate increased with bed pressure. It was noticed that the mean pierced

bubble length reported was about 0.12–0.45 m, which implied that the bed was almost in slugging fluidization when the bed cross-section was 0.2 m × 0.3 m.

Wiman et al. (1995) studied the hydrodynamics and tube erosion in different tube banks in a pressurized fluidized bed at constant $u_0 - u_{mf}$ and ambient temperature. They stated that there was a preferred bubble path along the tube-free centerline of the bed for an inline tube bank, which caused different erosion pattern between inline and staggered tube banks. Recently, Wiman and Almstedt (1997) found that the increased pressure caused a transition towards a dispersed bubbling, or turbulent bed behavior.

With respect to numerical studies on particle and bubble motions in a fluidized bed containing tube banks, previous investigators mainly dealt with cases at ambient conditions and few of them discussed the effects of bed pressure at high temperatures.

An approach to the issue from computer simulation was initiated by Lyczkowski et al. (1987, 1989). They presented a computer software package to predict the dynamics and erosion in fluidized bed tube banks by using a so-called two-fluid model. Their hydrodynamic model of fluidization was based on the conservation equations for mass and momentum, originally proposed by Anderson and Jackson (1967). However, in their model, the tubes had to be treated by rectangular objects due to the limitation of computer capacity. Ding and Lyczkowski (1992) extended the above model to simulate a three-dimensional bed.

Also based on the two-fluid model, Gustavsson and Almstedt (1998) developed a numerical code 'Gemini' with a curvilinear solver for the simulation of fluid dynamics in pressurized fluidized beds with horizontal tubes. They stated that in terms of mean bubble fraction, the experiment and the simulation were in good agreement over the pressure range of 0.1–1.6 MPa.

Generally speaking, the two-fluid model is capable of handling the bubble behavior around tubes by providing average bed voidage, but it can not provide any detailed information on particle–tube attacks.

However, a truly realistic computer simulation is now becoming possible with the development of discrete element method (DEM) which was initiated by Tsuji et al. (1993) for fluidized beds.

Rong et al. (1999) simulated an atmospheric fluidized bed containing tubes by extending the DEM based SAFIRE code. The bubble behavior predicted was verified by an experiment. They demonstrated that the DEM simulation is able to provide detailed information of particle and bubble behaviors around a tube, particularly particle–tube impact velocity, impact angle and the number of impacts which are indeed important to evaluate heat transfer and tube erosion.

In this paper, by using DEM, the direct simulation of a fluidized bed with a tube bank is extended to the cases at high temperature and pressure.

2. Theory

2.1. Governing equations and tube treatments

In the present simulation, the numerical model and computer code (SAFIRE ver.3) similar

to Rong et al. (1999) were adopted, except for taking into account the coupling of interactions between solid and gas phases.

The basic equations for fluid and particle–particle interaction were similar to those used by Tsuji et al. (1993) and Mikami et al. (1998) and the particle–fluid interaction was considered to meet the Newton's third law.

For fluid (gas) motion, the local averaged Navier–Stokes equations (Anderson and Jackson (1967) equations) were used.

$$\frac{\partial \varepsilon}{\partial t} + \nabla \cdot (\varepsilon u_g) = 0 \tag{1}$$

$$\frac{\partial (\rho_g \varepsilon u_g)}{\partial t} + \nabla \cdot (\rho_g \varepsilon u_g u_g) = -\varepsilon \nabla p + \beta (v - u_g) - \varepsilon \rho_g g \tag{2}$$

where g is the gravity, p is the gas pressure, u_g is the gas velocity, v is the particle velocity, β is the inter-phase momentum transfer coefficient, ε is the voidage fraction and ρ_g is the gas density.

When the void fraction (porosity) $\varepsilon < 0.8$, β can be obtained from Ergun equation as:

$$\beta = 150 \frac{(1-\varepsilon)^2}{\varepsilon} \frac{\mu}{d_p^2} + 1.75(1-\varepsilon) \frac{\rho_g}{d_p} |u_g - v| \tag{3}$$

where d_p is the particle diameter and μ is the gas viscosity.

When $\varepsilon > 0.8$, the Wen-Yu (1966) correlation is adopted:

$$\beta = \frac{3}{4} C_d \frac{\varepsilon (1-\varepsilon)}{d_p} \rho_g |u_g - v| \varepsilon^{-2.65} \tag{4}$$

where the drag coefficient C_d is a function of particle Reynolds number,

$$Re_p = \frac{|u_g - v|}{\mu} d_p \varepsilon \rho_g \tag{5}$$

$$C_d = \frac{24}{Re_p} \left(1 + 0.15 Re_p^{0.687}\right) \quad \left(Re_p < 1000\right) \tag{6}$$

$$C_d = 0.44 \quad \left(Re_p \geq 1000\right) \tag{7}$$

The particle motion is dependent on Newton's second law:

$$m_p \dot{\vec{v}} = \vec{F}_f + \sum \vec{F}_c + \vec{F}_g \tag{8}$$

where $\vec{F}_c$, $\vec{F}_f$, and $\vec{F}_g$ are the forces acting on a particle caused by collision, particle–fluid interaction force and gravity, respectively; m_p is the particle mass and $\dot{\vec{v}}$ is the acceleration of the particle.

The particle–particle collision force $\vec{F}_c$ is based on DEM, which can further be divided into

normal and tangential components: $\vec{F}_{cn}$ and $\vec{F}_{ct}$,

$$\vec{F}_{cn} = -k\vec{d}_n - \eta\vec{v}_n \tag{9}$$

$$\vec{F}_{ct} = -k\vec{d}_t - \eta\vec{v}_t \quad \left(|\vec{F}_{ct}| < \mu_f|\vec{F}_{cn}|\right) \tag{10}$$

$$\vec{F}_{ct} = -\mu_f|\vec{F}_{cn}| \cdot \left(\frac{\vec{v}_t}{|\vec{v}_t|}\right) \quad \left(|\vec{F}_{ct}| \geq \mu_f|\vec{F}_{cn}|\right) \tag{11}$$

where $\vec{d}_n$ and $\vec{d}_t$ are the particle displacement in normal and tangential directions, respectively; k is the spring constant; $\vec{v}_n$ and $\vec{v}_t$ are the particle velocity in normal and tangential directions; η is the coefficient of viscous dissipation; μ_f is the friction coefficient. Among them, the parameters k, η and μ_f have to be chosen. The spring constant k can be calculated by Hertz contact theory, which relates to the stiffness of particle surface. Here, to save the computation time, relatively soft particle stiffness was chosen because the dominant force causing particle motion is that of fluid (Tsuji et al., 1993). The spring constant k used in this work was 800 N/m, the friction coefficient μ_f was assumed to be 0.3 and η was determined by the restitution coefficient e ($e = 0.9$):

$$\eta = -2\ln e\sqrt{\frac{mk}{\pi^2 + \ln^2 e}} \tag{12}$$

The particle–fluid interaction force can be written as,

$$\vec{F}_f = -V_p\nabla p + \frac{1}{n}\beta(u_g - v) \tag{13}$$

where V_p is the particle volume and n is the number of particles in a fluid cell.

The tangential component of collision force acting on a particle, $\vec{F}_{ct}$, causes particle rotation. This rotation motion can be expressed as:

$$\dot{\vec{\omega}} = \frac{r_p\sum\vec{F}_{ct}}{I} \tag{14}$$

where I is the inertia moment of the particle, r_p is the particle radius and $\dot{\vec{\omega}}$ is the angular acceleration.

For tube treatment, as Rong et al. (1999) did, a tube was treated as a fixed circular obstacle for the calculation of particle–tube interaction. The movement of particles at the outer surface of a tube was classified as collision, rotation and sliding as illustrated in Fig. 1(a). The computation of particle–tube interaction was similar to that of particle–particle.

On the other hand, the tube boundary was approximated by staircase-like lines for the prediction of gas flow chart. The reason to choose such a non-curvilinear solver is to make it possible for the simulation of large amount of particles, while keeping the deviation and the duration of calculation within an acceptable region. As can be seen in Fig. 1(b), the tube area

was covered with square fluid cells which were maintained in proper size. This is because the fluid cell should be large enough to keep the calculation stable, (i.e. usually more than 10 particles in a cell); meanwhile, it should be as small as possible to make a close approximation of the round tube shape. Therefore, the ratio of tube diameter to cell size (Δx or Δy) was chosen as 10 and the ratio of cell size to particle diameter was 3.

The fluid cells were classified into three types, i.e. the tube-free cells, the boundary cells and the inside-tube cells. The so-called boundary cells are those which contact with the outside arc of the round tube. Furthermore, if the center of a boundary cell is within the tube area, it is defined as an "inside-boundary cell"; otherwise it is defined as an "outside-boundary cell". For each inside boundary cell, it was assumed that there was no gas flowing into and out of the cell; whereas for the calculation of particle motions in such a cell, the gas velocity had to be generated by interpolating the data of its neighboring cells. For each outside boundary cell, it was treated that the gas did not pass through the tube side edges. In addition to calculating the gas velocity in an outside boundary cell, the equivalent bed voidage in the cell was obtained by assuming that the tube area in a cell was filled with particles of a fixed bed voidage, 0.48, because, by doing so, the calculated gas drag force can be close to the real drag force (Rong et al., 1999). On the other hand, the bed voidage around a tube (the voidage of a tube-free or boundary cell) shown in this paper is the real voidage determined by

$$\varepsilon = 1 - \sum V_{\mathrm{p}}/(V_{\mathrm{cell}} - V_{\mathrm{tube}}) \tag{15}$$

where $\sum V_{\mathrm{p}}$ is the amount of particle volume in a cell, V_{cell} is the volume of a square cell and V_{tube} is the volume of tube region within the cell.

2.2. Computation conditions

The computing conditions are listed in Table 1.

A fluidized bed shown in Fig. 2 was simulated to analyze the effect of bed pressures (0.1, 0.5, and 1.2 MPa) on particle and bubble motions around immersed tubes at high temperature, 850°C. A tube bank was immersed in the bed of 0.33 m in width and 0.99 m in height. The diameter of each tube was 30 mm. Tubes were placed in five rows with vertical and horizontal

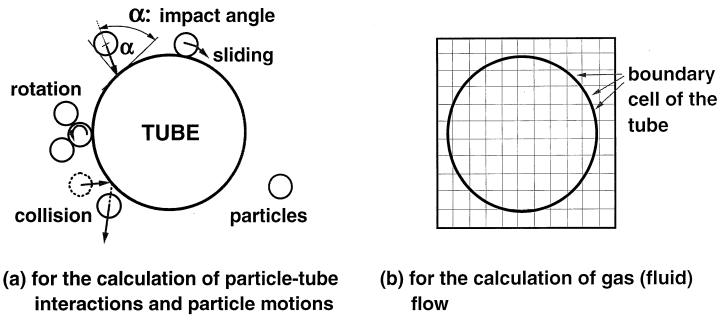

Fig. 1. Treatment of a tube for the DEM simulation.

Table 1
Computing conditions

Bed/distributor/tube	
Width (m)	0.33
Height (m)	0.99
Orifice diameter (mm)	3
Orifice number	28
Tube arrangement	Staggered
Tube diameter (mm)	30
Tube number	23
Particle	
Particle number	140,000
Particle density (kg/m^3)	2650
Particle shape	Sphere
Particle diameter (mm)	1
Gas	
Gas viscosity (Pa s)	4.55E−5
Gas density (kg/m^3)	0.314, 1.57, 3.77
Gas pressure (MPa)	0.1, 0.5, 1.2
Minimum fluidization velocity u_{mf} (m/s)	0.52, 0.42, 0.34
Computing	
Cell width Δx (mm)	3
Cell height Δy (mm)	3
Time step (s)	2.58E−5
DEM	
Restitution coefficient, e	0.9
Spring constant, k (N/m)	800
Friction coefficient, μ_f	0.3

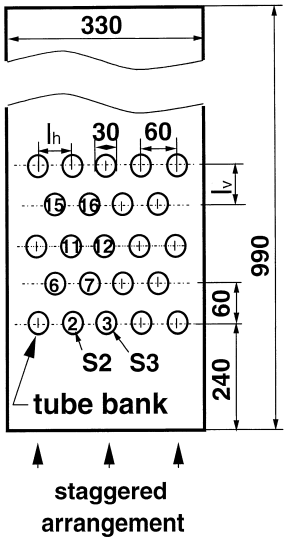

Fig. 2. A simulated fluidized bed and tube bank.

spacing, l_v and l_h, respectively, of 60 mm. The centers of the bottom row tubes were located 240 mm above the distributor (Fig. 2).

Computation was done for 4.64 s (real). The simulated bed was initially at the fixed bed condition. During the first 0.2 s, the superficial velocity of fluidizing gas was increased linearly from 0 to u_0, and then the gas velocity was kept constant. In the case of $P = 1.2$ MPa and $u_0 = 0.50$ m/s, it took less than 1.5 s for the initial large bubble passing through the tube bank and making particles and small bubbles spread smoothly in the bed. In other cases, the time duration for smooth dispersing of particles and small bubbles was shorter than the former case. Accordingly, the calculations of particle–tube attack and bubble motion were based on the last 3 s (1.64–4.64 s) when the bed was in a stable fluidization condition with a bubble frequency of 4–8 Hz, so that statistical averages can be allowable in a certain degree.

Particle–tube impact velocity, impact angle (Fig. 1(a)), impact site, the number of impacts, and the bed voidage around a tube were calculated to investigate the particle effect on tubes. The impact velocity was defined as the particle velocity at the previous time step right before a particle–tube contact occurred. The bed voidage around a tube was calculated based on the tube-free part of boundary cells.

The CPU time for the calculation of one real second was about 90 h when using a HP 9000 C160 workstation.

3. Computational results and discussions

To evaluate the motion of particles and bubbles in a fluidized bed at elevated pressure and high temperature, the criterion for comparison has to be chosen. Constant $u_0 - u_{mf}$ or u_0/u_{mf} is usually selected for such a comparison (Glicksman et al., 1991). In this case, the bed expansion height should be one of the most important parameters for the judgement. Assuming that the dense phase region is the region where cross-section averaged voidage is less than 0.8, the bed expansion height can be identified. In our simulation (Fig. 3), bed voidage was cross-section averaged along the bed height over 3 s to obtain time averaged bed expansion height L_{exp}. Here, the tube area was excluded from the computational domain. As shown in Fig. 3, at 0.5 MPa, the bed expansion based on constant $u_0 - u_{mf}$ was about 0.53 m, higher than that based on constant u_0/u_{mf}, 0.50 m. At 1.2 MPa, the bed expansion based on constant $u_0 - u_{mf}$ and u_0/u_{mf} were roughly 0.54 m and 0.52 m, respectively. It is clear that the bed expansion height at constant u_0/u_{mf} was closer to the initial bed expansion height than that at constant $u_0 - u_{mf}$. Accordingly, in present calculation, u_0/u_{mf} was maintained constant for comparison of bubble and particle behaviors at different pressure conditions.

3.1. Bubble behavior

Fig. 4 illustrates the visible bubble flow pattern in a bed containing a staggered tube bank at high temperature under different set of pressure ranges. It can be found that in the tube bank regions, bubble number increases and the bubbles become relatively small at elevated pressures 0.5 and 1.2 MPa. This is dependent on the balance between bubble coalescence and splitting. Usually, with the increasing pressure, both bubble coalescence and splitting are increased for a

freely bubbling bed, and at a higher pressure, bubble splitting is the dominant (Hoffmann and Yates, 1986). In the present case, the existence of tubes in staggered arrangement enhanced the bubble splitting, and as a result, the bubble splitting governed the bubble behavior, the bubble size decreased and the number of bubbles increased at elevated pressures. The calculated results are consistent with the previous experimental findings (Olsson et al., 1995; Wiman et al., 1995) in terms of bubble behavior at elevated pressures.

Fig. 5 illustrates the average voidage of each computing cell in the bed. Here, each tube center was given a constant voidage ($\varepsilon = 0.1$), so that it could be easily distinguished by its color in the figure. It can be seen that the voidage in the tube bank region is generally 0.5–0.6, while it is about 0.4–0.5 in the regions near the vertical wall. Also, it can be found that the voidage around a tube is relatively high, i.e. greater than 0.6. As shown in Fig. 5, there are some regions with voidage 0.6–0.7 in the center of the tube bank at elevated pressures, 0.5 and 1.2 MPa. This implies that the bubble fractions increased in the center of the bed with the increasing pressure.

The effect of bed pressure on bed expansion can be found in Fig. 3. At 0.1 MPa, the bed expansion height L_{exp} is about 0.48 m, whereas it is around 0.50 m at 0.5 MPa and 0.52 m at 1.2 MPa, respectively. It is clear that the bed expansion height increases with increasing bed pressure at a constant u_0/u_{mf}.

In Fig. 6, the present data of bed expansion results are compared with those calculated from the Lofstrand et al. (1995) correlation given in Appendix A. In their correlation, immersed tube bank effect, bed pressure and temperature can be taken into account, although the cases of high temperatures have not been examined enough.

It can be seen in Fig. 6 that the bed expansion height predicted by the correlation increases with the increase of pressure. This tendency is in agreement with our DEM simulation. The

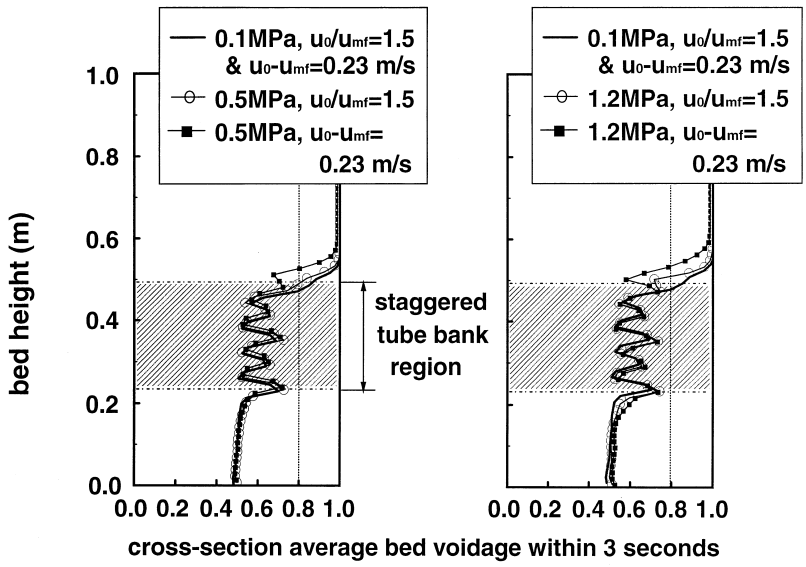

Fig. 3. Comparison of bed expansion height between constant $u_0 - u_{\mathrm{mf}}$ and u_0/u_{mf}.

bed expansion height predicted by our simulation is higher than that predicted by the correlation. This is probably due to the different definition of bed height. It is noticed that the average bed height was defined from a linear extrapolation of the pressure drop (assumed to be relatively constant through the bed by Lofstrand et al. (1995)) to the freeboard pressure.

3.2. Particles motion around the tubes

Concerning the bed containing a staggered tube bank operated at 850°C under 0.1 and 1.2 MPa, Fig. 7 shows all the computed particle–tube impacts onto the tube bottom area (i.e. $\pm 2^{\circ}$ from the tube bottom center) for tubes S3, S7 and S12 over the 0.5 s period between 3.1 and 3.6 s, in terms of bed voidage, particle–tube impact velocity and impact angle. As already defined in Fig. 2, tubes S3 and S12 are located on the centerline of the tube bank, the former belongs to the bottom row and the latter to the third row. Tube S7 is located at the second row and 1/2 pitch from the centerline. In Fig. 7, it can be found that the periodical peaks in the voidage response correspond to the bubble passage if they are compared with Fig. 4. For instance, in Fig. 4, there is one bubble passing around the tube S3 in the period of "a" to "e"

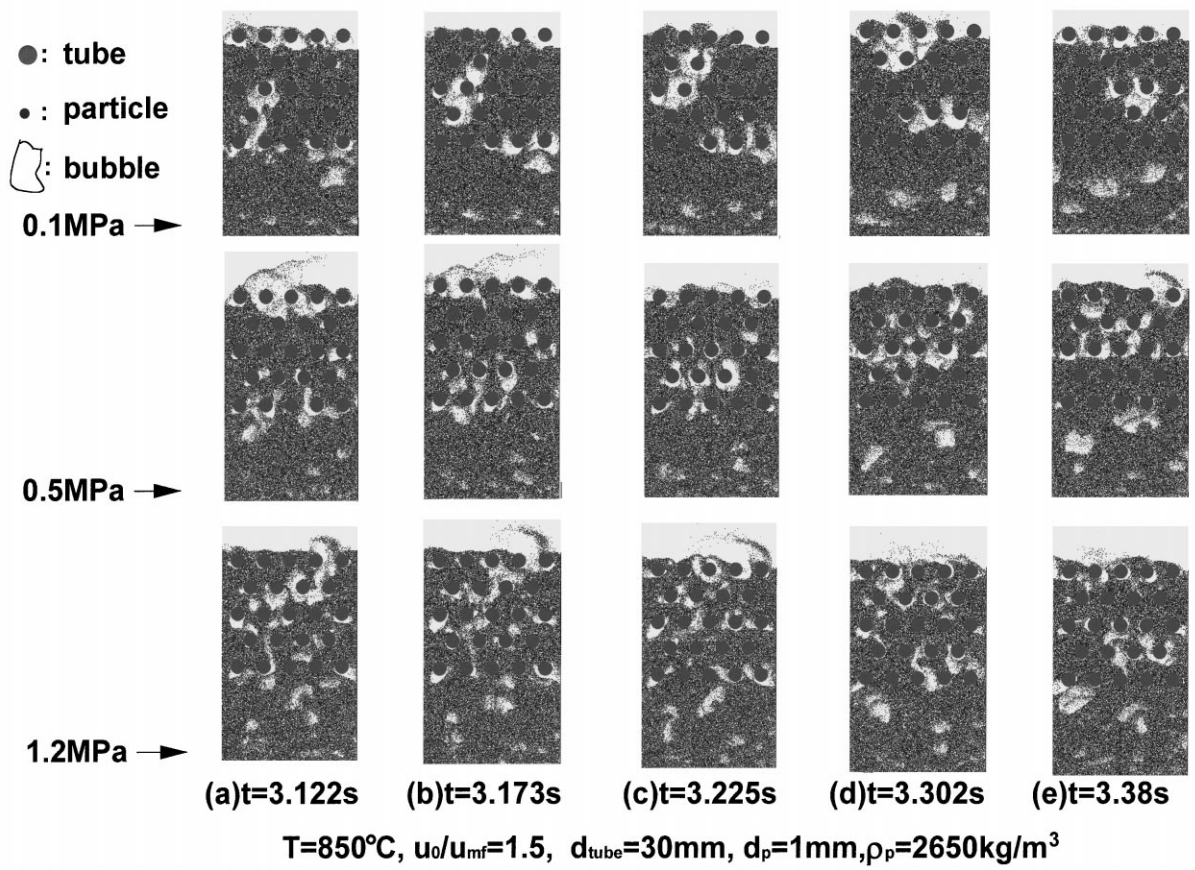

Fig. 4. Numerical snapshots for staggered tube banks.

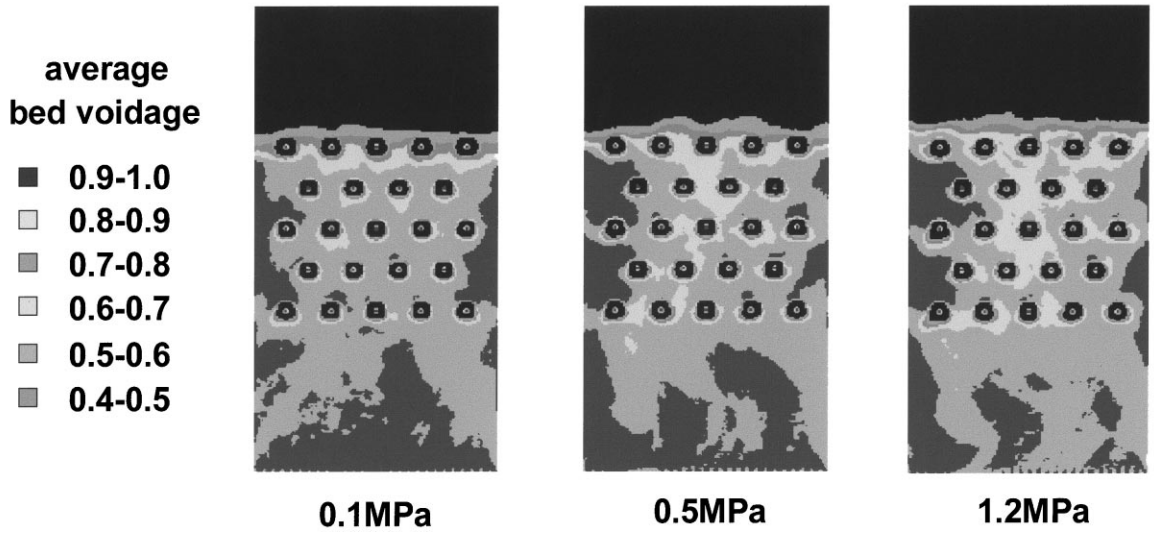

Fig. 5. Average bed voidage of each computing cell in the whole bed at 850°C and different pressures (within 3 s).

at 0.1 MPa, while there is a peak of voidage ε up to 1 in Fig. 7(a) for tube S3 at the same time. The frequency of the ε fluctuation is roughly 4 Hz at 0.1 MPa for Fig. 7(a) and 4–8 Hz at 1.2 MPa for Fig. 7(b), being slightly higher than what Rong et al. (1999) obtained from ambient conditions, 2–4 Hz.

It can be also found from Fig. 7 that the impact velocity and impact angle varies over a wide range, and the particle impacts are concentrated during the period of bubble wake attacks. Similar results are obtained in our simulation for an atmospheric fluidized bed.

The time averaged particle–tube impact velocity and impact angle are shown in Fig. 8 for tubes S3, S7 and S12. The average impact velocity for $P = 1.2$ MPa generally shows higher

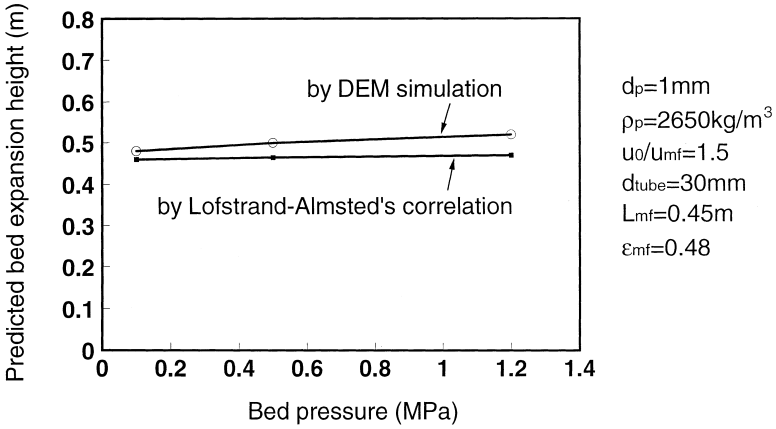

Fig. 6. Comparison of bed expansion height predicted by DEM simulation and the correlation of Lofstrand et al. (1995).

values than for cases of lower pressures. However, for $P = 0.1$ and 0.5 MPa, the effect of pressure on the average impact velocities is not obvious. For instance, the average impact velocities for tube S7 do not change much at $P = 0.1$ and 0.5 MPa. The maximum of the average impact velocity can be found at the positions between 10° and 70° from tube bottom center for each tube at $P = 0.1$–1.2 MPa. With respect to the average impact angle, the maximum value appears near the bottom of each tube, which increases with the increasing pressure. It can be seen from Fig. 8, the distribution of average impact velocity and impact angle are asymmetric for the left and right halves of a tube. This asymmetry is probably due to the bubble passage habit and the short duration of our computation time.

Fig. 9 illustrates the time-averaged voidage around tubes S3, S7 and S12 for different bed pressures. It can be seen that the distribution of average voidage is asymmetric for all the tubes examined, and the average voidage increases with the increasing pressure. In the cases of 0.1 and 0.5 MPa, the average voidage reaches its minimum (i.e. around 0.7) at the tube top area and its maximum (i.e. above 0.9) at the bottom area. However, in the case of S3 at 1.2 MPa, the point of maximum voidage (i.e. about 0.97) shifts to the right side, about 60° from the tube bottom. In the cases of S7 and S12 at 1.2 MPa, the maximum voidages (i.e. roughly 0.93 and 0.98, respectively) shift further to 90° at right and left sides.

The characteristics of voidage behavior for each tube mentioned above could be explained

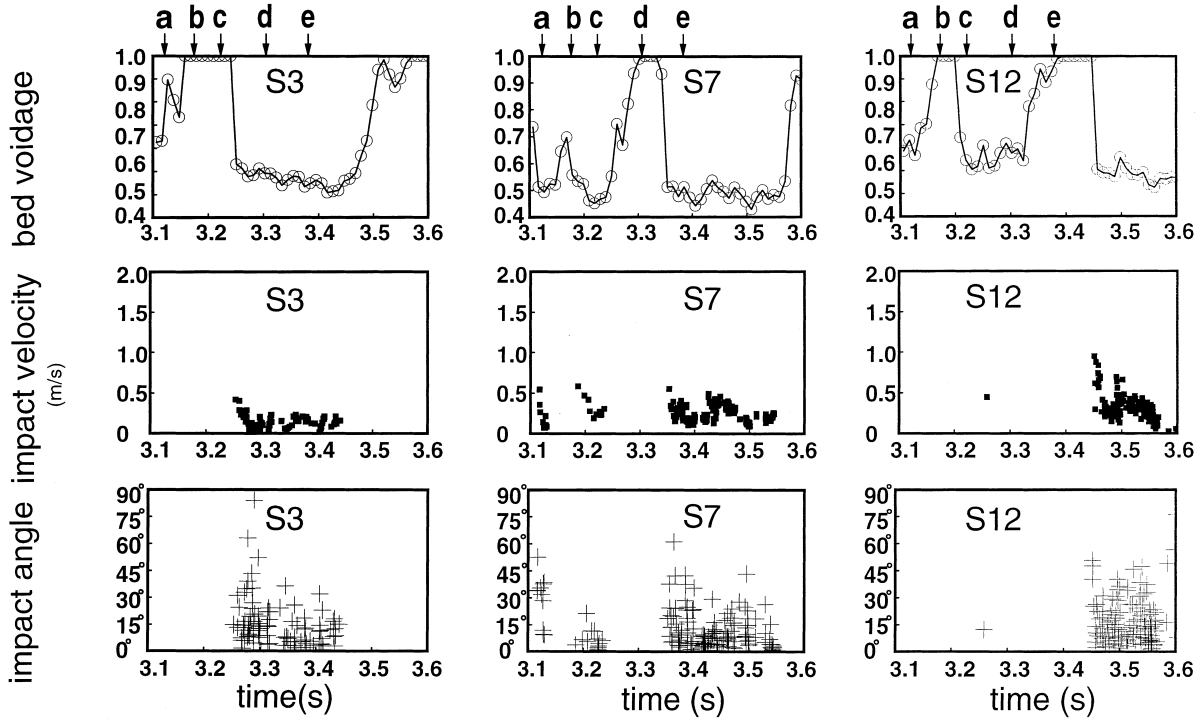

Fig. 7. (a) Bed voidage, impact velocity and impact angle vs. time in a staggered tube bank.

by comparing Figs. 9 and 5. From the time-averaged voidage of each cell in the whole bed shown in Fig. 5, we can find the bubble passage habit. For instance, at $P = 1.2$ MPa, high voidage ($\varepsilon > 0.6$) regions exist at the right side of tubes S3 and S7, and at the left side of tube S12. On the other hand, at $P = 0.1$ and 0.5 MPa, such high voidage regions can not be distinguished. This implies that the bubble passage habit was changed with the pressure due to the change in bubble characteristics.

In order to obtain the tube erosion rate, Finnie's erosion model (Finnie, 1960) was adopted. In this model, the volume removed by one impact was correlated as

$$W = 0.125 m v_p^2 f(\alpha)/P_H \tag{16}$$

$$f(\alpha) = \sin 2\alpha - 3\sin^2\alpha, \quad \alpha \leq 18.43^\circ \tag{17}$$

$$f(\alpha) = 1/3\cos^2\alpha, \quad \alpha > 18.43^\circ \tag{18}$$

where m is the particle mass, P_H is the Vickers hardness of the target surface, v_p the particle velocity, W is the volume removed by one particle–tube impact and α is the impact angle. Among them, P_H was chosen as 6×10^8 kg/m^2 as Stringer et al. (1989) suggested.

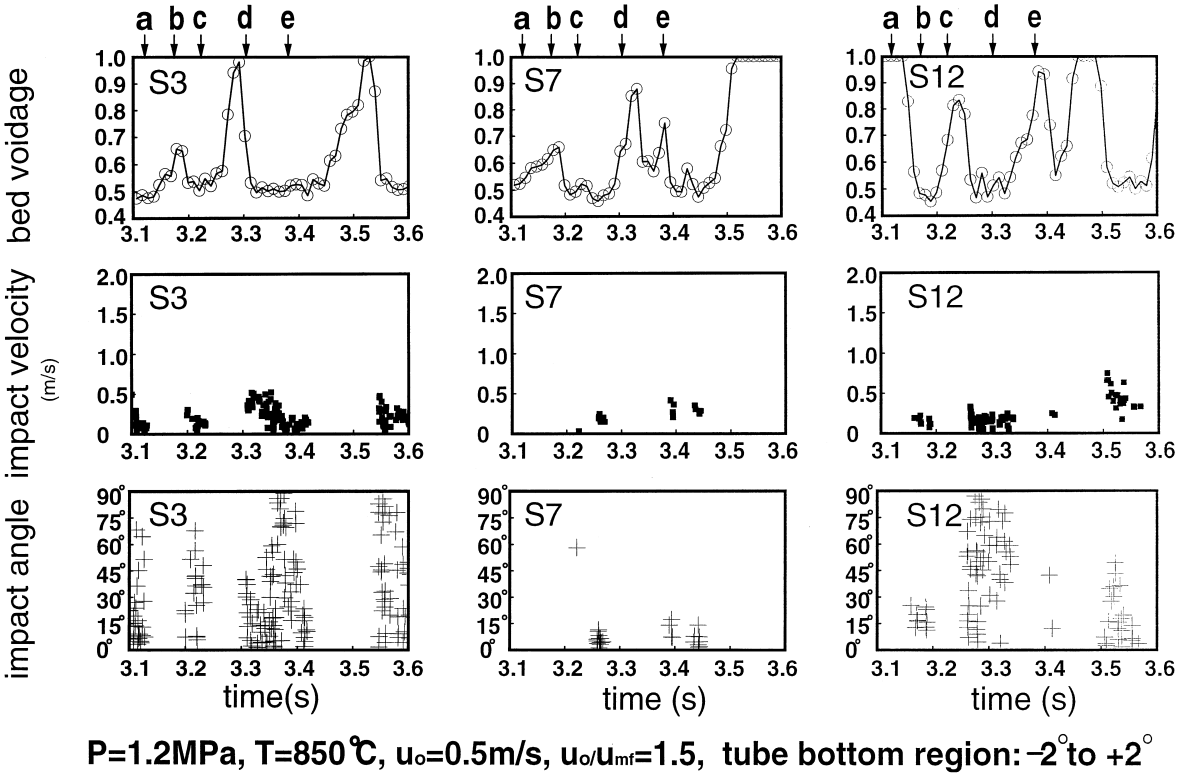

Fig. 7. (b) Bed voidage, impact velocity and impact angle vs. time in a staggered tube bank.

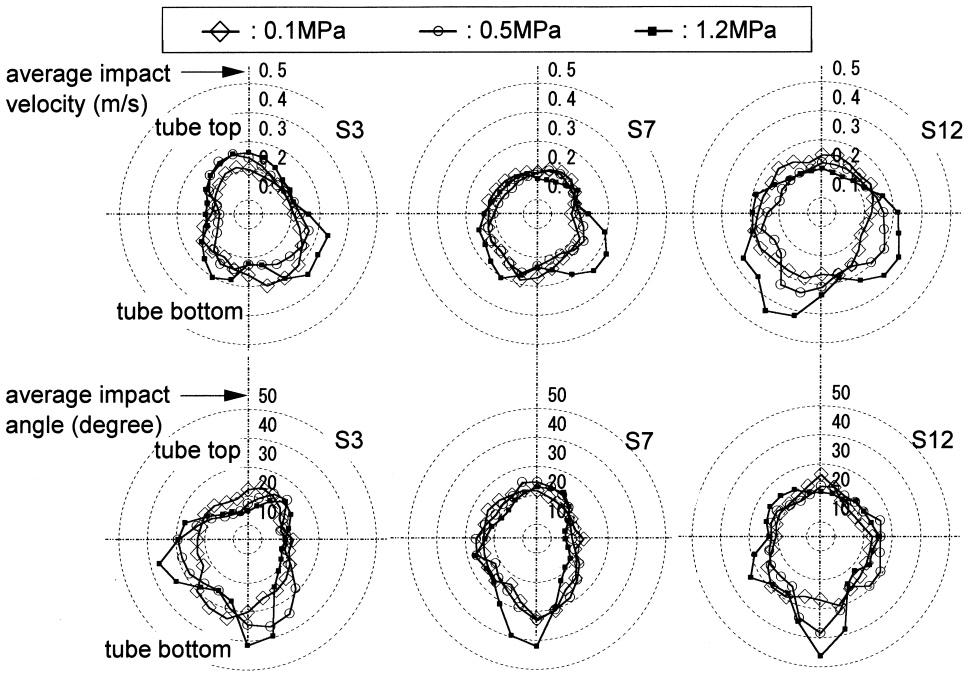

Fig. 8. Average impact velocity and impact angle around a tube at different pressures (within 3 s).

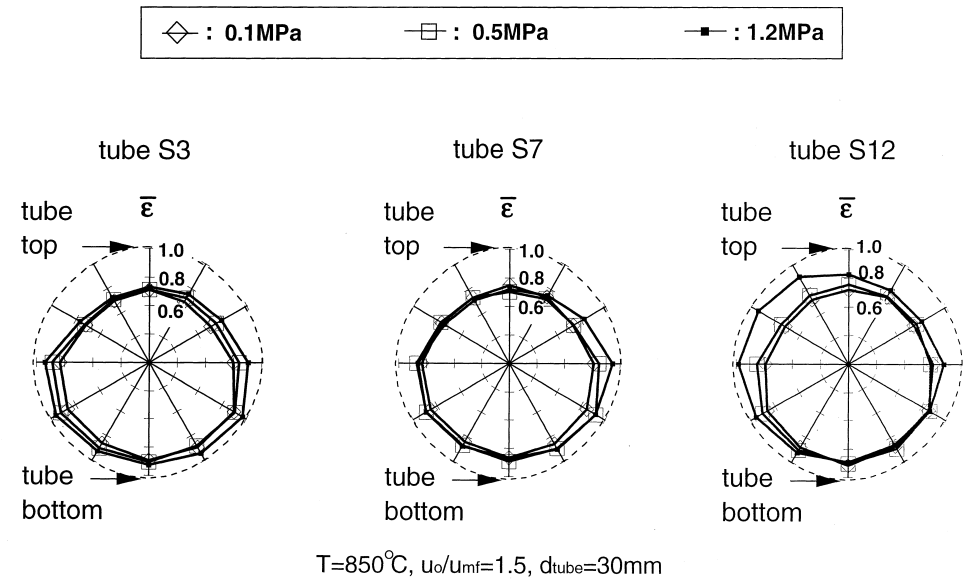

Fig. 9. Effect of bed pressure on average voidage around a tube (within 3 s).

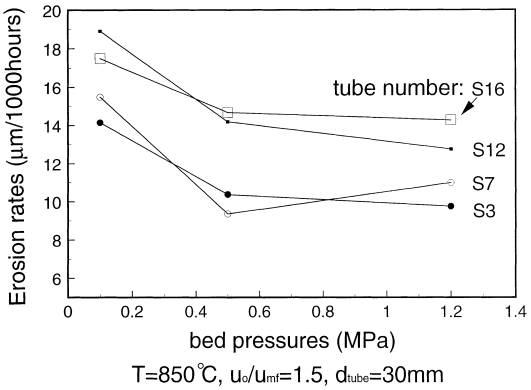

Fig. 10. Effect of bed pressure on tube erosion rates (within 3 s).

Therefore, the time averaged erosion rate, E_t (μm/1000 h), can be calculated as follows

$$E_t = 3600 \times 10^9 \cdot \sum W/(A_t \cdot \Delta t_c) \tag{19}$$

$$A_t = \pi d_{tube} d_p \tag{20}$$

where Δt_c is the time duration, D_t is the tube diameter and d_p is the particle diameter.

Fig. 10 shows the effect of bed pressure on tube erosion rates, in which the tubes S3, S7, S12 and S16 are located in different tube rows along the bed height, respectively. The erosion rates are within 7.9–19.4 μm/1000 h. It is interesting to find that the erosion rates of the sampled tubes have their maximums at ambient pressure when keeping u_0/u_{mf} constant. This is due to the contribution of a large amount of particle impacts at ambient pressure, although the time-averaged particle tube impact velocity is not as high as that at elevated pressure, i.e. 1.2 MPa. The erosion rates of tubes S3 and S7, which are located in the bottom and the second rows, are lower than those of tubes S12 and S16 in the third and the fourth rows. It is noticed (see Fig. 5) that the gas–solid flow patterns in the bed-bottom and the tube bank regions are different, partly due to the change of effective cross-section area. The transition of the flow patterns may occur near the two bottom tube rows. As a result, the gas–solid flow near the two bottom rows is not as fierce as that near the upper tube rows, which leads to the small value of erosion rates for tubes in the two bottom rows.

4. Conclusions

The discrete element method (DEM) was applied to simulate the behavior of particles and bubbles around the tubes in a pressurized fluidized bed at high temperature.

At constant u_0/u_{mf}, bed expansion height increased with the increasing bed pressure. At elevated pressures, bubble size was reduced while bubble number was increased particularly in the tube bank region. At 1.2 MPa, the bubble frequency was roughly 4–8 Hz, slightly higher than that (2–4 Hz) at ambient condition. The average particle–tube impact velocity at $P = 1.2$

MPa was generally higher than that at $P = 0.1$ or 0.5 MPa. The maximum of average impact velocity corresponded to the position of 10–70° from the tube bottom. Such particle–tube impacts were concentrated during the period of bubble wake attack on each tube both at ambient and elevated pressures. The average particle–tube impact angle was found to reach its maximum near the tube bottom. The average bed voidage around a tube was asymmetric and the position of maximum voidage shifted upward from tube bottom center with the pressure increasing, which are because of the change in local bubble habits. The tube erosion rate predicted was 7.9–19.4 μm/1000 h and the maximum erosion rate occurred at ambient pressure.

Appendix A. Lofstrand et al. (1995) correlation for bed expansion

In this correlation, bed expansion ratio δ is related to a function of a dimensionless drag force F^* and a dimensionless horizontal and vertical tube pitch function S.

$$\delta \equiv \frac{L_{\mathrm{exp}} - L_{\mathrm{mf}}}{L_{\mathrm{mf}}} = 0.11(F^* - 1)^{0.34S} \tag{A1}$$

where

$$F^* = \frac{F_{\mathrm{D}}}{m_{\mathrm{p}} g} = \frac{1}{1-\varepsilon_{\mathrm{mf}}} \frac{1}{g\rho_{\mathrm{p}}} \left[\frac{\Delta P}{H}\right]_{\varepsilon=\varepsilon_{\mathrm{mf}}} = \frac{Re}{\varepsilon_{\mathrm{mf}} Ar}\left[150\frac{1-\varepsilon_{\mathrm{mf}}}{\varepsilon_{\mathrm{mf}}} + 1.75Re\right]$$

$$Re \equiv \frac{d_{\mathrm{p}} u_0 \rho_{\mathrm{g}}}{\varepsilon_{\mathrm{mf}}\mu} \quad \text{and} \quad Ar \equiv \frac{d_{\mathrm{p}}^3 \rho_{\mathrm{p}} \rho_{\mathrm{g}} g}{\mu^2}$$

S is chosen as:

$$S = \left(\frac{W}{W - N_{\mathrm{h}} d_{\mathrm{tube}}}\right)^{0.89} \cdot \left(\frac{\bar{H}_{\mathrm{fl}}}{\bar{H}_{\mathrm{fl}} - N_{\mathrm{v}} d_{\mathrm{tube}}}\right)^{0.27}$$

d_{tube} is tube diameter, $\bar{H}_{\mathrm{fl}}$ is the time averaged bed height, L_{exp} is the bed expansion height, L_{mf} is the bed height at minimum fluidization, N_{h} and N_{v} are the average number of tubes in the horizontal and vertical direction, respectively, W is the bed width, $\varepsilon_{\mathrm{mf}}$ is the bed voidage at minimum fluidization.

References

Anderson, T.B., Jackson, R., 1967. A fluid mechanical description of fluidized beds. I & EC Fundamentals 6, 527–539.

Botterill, J.S.M., Desai, M., 1972. Limiting factors in gas-fluidized heat transfer. Powder Technology 6, 231–238.

Chan, I.H., Shishtla, C., Knowlton, T.M., 1987. The effect of pressure on bubble parameters in gas fluidized beds. Powder Technology 53, 217–235.

Ding, J., Lyczkowski, R.W., 1992. Three-dimensional kinetic theory modeling of hydrodynamics and erosion in fluidized beds. Powder Technology 73, 127–138.

Finnie, I., 1960. Erosion of surface by solid particles. Wear 3, 87–103.

Glicksman, L.R., Yule, T., Dyrness, A., 1991. Prediction of the expansion of fluidized beds containing tubes. Chem. Engng. Sci 46, 1561–1571.

Gustavsson, M., Almstedt, A.E., 1998. Numerical simulation of fluid dynamics in fluidized beds with horizontal heat exchanger tubes. Thesis for the degree of Licentiate of Engineering, Department of Thermo and Fluid Dynamics, Chalmers University of Technology.

Hoffmann, A.C., Yates, J.G., 1986. Experimental observations of fluidized beds at elevated pressures. Chem. Engng. Commun. 41, 133–149.

Kawabata, J., Yumiyama, M., Tazaki, Y., Honma, S., Chiba, T., Sumiya, T., Endo, K., 1981. Characteristics of gas fluidized beds under pressure. J. Chem. Engng. Japan 14, 85–89.

Knowlton, T.M., 1977. High pressure fluidization characteristics of several particulate solids: primarily coal and coal-derived materials. A.I.Ch.E. Symp. Ser 73 (161), 22–28.

Lofstrand, H., Almstedt, A.E., Andersson, S., 1995. Dimensionless expansion model for bubbling fluidized beds with and without internal heat exchanger tubes. Chem. Engng. Sci. 50, 245–253.

Lyczkowski, R.W., Bouillard, J.X., Berry, G.F., 1987. Erosion calculations in a two-dimensional fluidized bed. In: Proceedings of the 9th International Conference on Fluidized Bed Combustion, Boston, 697–706.

Lyczkowski, R.W., Folga, S., Chang, S.L., Bouillard, J.X., Wang, C.S., Berry, G.F., Gidaspow, D., 1989. State-of-the-art computation of dynamics and erosion in fluidized bed tube banks. In: Proceedings of the 10th International Conference on Fluidized Bed Combustion, San Francisco, 465–478.

Mii, T., Yoshida, K., Kuni, D., 1973. Temperature effects on the characteristics of fluidized beds. J. Chem. Engng. Japan 6, 100–102.

Mikami, T., Kamiya, H., Horio, M., 1998. Numerical simulation of cohesive powder behavior in a fluidized bed. Chem. Engng. Sci 53, 1927–1940.

Olowson, P.A., Almstedt, A.E., 1990. Influence of pressure and fluidization velocity on the bubble behavior and gas flow distribution in a fluidized bed. Chem. Engng. Sci 45, 1733–1741.

Olsson, S.E., Wiman, J., Almstedt, A.E., 1995. Hydrodynamics of a pressurized fluidized bed with horizontal tubes: influence of pressure, fluidization velocity and tube-bank geometry. Chem. Engng. Sci 50, 581–592.

Otake, T., Tone, S., Kawashima, M., Shibata, T., 1975. Behavior of rising bubbles in a gas-fluidized bed at elevated temperature. J. Chem. Engng. Japan 8, 388–392.

Rong, D.G., Mikami, T., Horio, M., 1999. Particle and bubble movements around tubes immersed in fluidized beds: a numerical study. Chem. Engng. Sci 54, 5737–5754.

Rowe, P.N., Foscolo, P.U.A., Hoffmann, C., Yates, J.G., 1983. X-ray observation of gas fluidized beds under pressure. In: Kunii, D., Toei, R. (Eds.), Fluidization. Engineering Foundation, New York, pp. 53–60.

Stringer, J., Stallings, J.W., Wheeldon, J.M., 1989. Wastage in bubbling fluidized-bed combustors: An update. In: Proceedings of the 10th International Conference on Fluidized Bed Combustion, New York, 857–862.

Tsuji, Y., Kawaguchi, T., Tanaka, T., 1993. Discrete particle simulation of two-dimensional fluidized bed. Powder Technology 77, 79–87.

Wen, C.Y., Yu, Y.H., 1966. A general method for predicting the minimum fluidization velocity. AIChE J. 12, 610–612.

Wiman, J., Mahpour, B., Almstedt, A.E., 1995. Erosion of horizontal tubes in a pressurized fluidized bed: influence of pressure, fluidization velocity and tube-bank geometry. Chem. Engng. Sci 50, 3345–3356.

Wiman, J., Almstedt, A.E., 1997. Hydrodynamics, erosion and heat transfer in a pressurized fluidized bed: influence of pressure, fluidization velocity, particle size and tube bank geometry. Chem. Engng. Sci 52, 2677–2695.

Yoshida, K., Ueno, T., Kunii, D., 1974. Mechanism of bed to wall heat transfer in a fluidized bed at high temperatures. Chem. Engng. Sci 29, 77–82.